Temperature-dependent photoluminescence on organic–inorganic metal halide perovskite $CH_3NH_3PbI_{3-x}Cl_x$ prepared on ZnO/FTO substrates using a two-step method*

Shiwei Zhuang(庄仕伟), Deqian Xu(徐德前), Jiaxin Xu(徐佳新), Bin Wu(伍斌), Yuantao Zhang(张源涛), Xin Dong(董鑫), Guoxing Li(李国兴), Baolin Zhang(张宝林)†, and Guotong Du(杜国同)

State Key Laboratory on Integrated Optoelectronics, College of Electronic Science and Engineering, Jilin University, Changchun 130012, *China*

(Received 27 August 2016; revised manuscript received 13 October 2016; published online 22 December 2016)

Temperature-dependent photoluminescence characteristics of organic-inorganic halide perovskite $CH_3NH_3PbI_{3-x}Cl_x$ films prepared using a two-step method on ZnO/FTO substrates were investigated. Surface morphology and absorption characteristics of the films were also studied. Scanning electron microscopy revealed large crystals and substrate coverage. The orthorhombic-to-tetragonal phase transition temperature was $\sim$ 140 K. The films' exciton binding energy was 77.6 ± 10.9 meV and the energy of optical phonons was 38.8 ± 2.5 meV. These results suggest that perovskite $CH_3NH_3PbI_{3-x}Cl_x$ films have excellent optoelectronic characteristics which further suggests their potential usage in perovskitebased optoelectronic devices.

Keywords: perovskite, temperature-dependent photoluminescence, two-step method, ZnO

PACS: 78.20.−e 78.55.−m **DOI:** 10.1088/1674-1056/26/1/017802

1. Introduction

Recently, organometal halide perovskite ABX_3 (A = organic cation, B = metal cation, X = halogen anion) materials have gained popularity in the field of photoelectrics, owing to their remarkable characteristics.[1–7] Perovskite has a tunable direct bandgap in the visible to the infrared range (390–790 nm).[1] The transport characteristics of both electron and hole carriers in this material are excellent.[2] In addition, perovskite exhibits high photoelectric conversion efficiency and high luminescence efficiency.[3] Perovskite-based solar cells are promising owing to a rapid increase in their power conversion efficiency (PCE) which increased from 3.8% to 20.1% in the last six years.[8–10] Perovskite-based lightemitting devices (LEDs), field effect transistors, and photodetectors with good performance have been reported.[11–13] Undoubtedly, organometal halide perovskites are among the most promising photoelectric materials. However, despite this promise, some fundamental issues still need to be addressed. For example, insufficient information is available about the role of organic cations in hybrid halide perovskites and about the mechanism underlying their high PCE. In addition, temperature dependence of photoactivated excitons remains poorly characterised. This makes it necessary to investigate the cryogenic photoluminescence characteristics of these materials.

As a third generation semiconductor, ZnO is a very stable material with good photoelectric characteristics.[14] It can be used as the electron transport layer in solar cells. In particular, one-dimensional ZnO nanorods have an excellent electron transport capability.[4,5,15,16]

In this study, temperature-dependent PL measurements of lead halide perovskites CH3NH3PbI$_{3-x}$Cl$_x$ on ZnO nanorods prepared using a two-step method were performed to determine the cryogenic photoluminescence characteristics and exciton binding energy of these materials, which should be useful for fabrication of future devices.

2. Experiments

The perovskite $CH_3NH_3PbI_{3-x}Cl_x$ samples were prepared using a two-step method. First, substrates were cleaned ultrasonically with a sequence of methylbenzene, acetone and alcohol. $PbCl_2$ (99.999% pure obtained from Sigma Aldrich) was deposited on the ZnO/FTO substrates (FTO: Fdoped SnO_2 conducting glass) using thermal evaporation. The evaporation rate was 0.1 nm/s and the film thickness was monitored using a TDM-200 film monitor. Subsequently, the precursor films were dipped into a solution of organo-ammonium halide CH_3NH_3I (MAI), with 8 mg/ml of isopropanol (IPA). After the reaction between $PbCl_2$ and MAI for 60 min, excess MAI was gently rinsed by IPA. Finally, the perovskite films were annealed at 90 °C for 30 min on a hot plate.

ZnO nanorods were prepared on FTO substrates under an optimised condition using metal-organic chemical vapour deposition (MOCVD) with diethylzinc (DEZn) and ultrahigh purity oxygen as the precursors. The deposition details were reported in our previous paper.[17] The FTO substrates were cleaned with acetone, ethanol and deionized water in this sequence at room temperature.

The morphology of the obtained perovskite

*Project supported by the International Science and Technology Cooperation Program of Science and Technology Bureau of Changchun City, China (Grant No. 12ZX68).

†Corresponding author. E-mail: zbl@jlu.edu.cn

© 2017 Chinese Physical Society and IOP Publishing Ltd

$CH_3NH_3PbI_{3-x}Cl_x$ samples was characterized by scanning electron microscopy (SEM) using a Jeol-7500F microscope. Photoluminescence (PL) spectra were acquired using a HORIBA iHR550 monochromator/spectrograph. Absorption spectra were obtained using a Shimadzu UV-VIS-NIR spectrophotometer UV-3600. A continuous 325 nm wavelength He–Cd laser from Kimmon was used as the excitation source. The laser power density on the film surface was ~ 1000 mW/cm^2. Temperature-dependent photoluminescence measurements were performed for temperatures in the 10–300 K range. All other measurements were performed at room temperature.

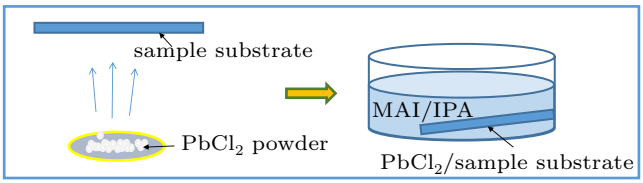


Fig. 1. (color online) Schematic of the synthesis of the perovskite $CH_3NH_3PbI_{3-x}Cl_x$ samples using a two-step method.

3. Results and discussion

Figure 2(a) shows ZnO nanorods on a FTO substrate. The diameters of the nanorods were in the 100–300 nm. This morphology was typical for ZnO nanorods grown on FTO substrates using MOCVD. Figure 2(b) shows the surface morphology of a perovskite $CH_3NH_3PbI_{3-x}Cl_x$ film deposited on a ZnO/FTO substrate. The coverage of the substrate layer is high and the crystal grains are very large. The morphology obtained using the two-step method was similar to that obtained previously.[18–20] As can be seen from the inset of Fig. 2(b), there are nanorods on the ZnO substrate. This film-nanorods structure can affect the photoelectric behaviour, which will be discussed later.

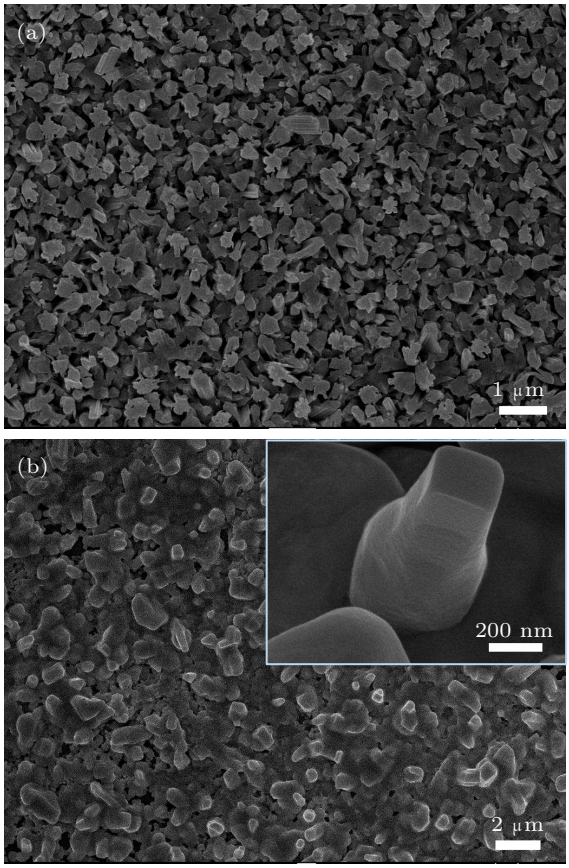


Fig. 2. (a) Top view of the surface morphology of the ZnO nanorods deposited on the FTO substrates. (b) Top view of the surface morphology of the perovskite $CH_3NH_3PbI_{3-x}Cl_x$ film deposited on the ZnO layer. The inset shows a $CH_3NH_3PbI_{3-x}Cl_x$ rod on the perovskite film.

Figure 3(a) shows the PL spectrum of $CH_3NH_3PbI_{3-x}Cl_x$ at room temperature. The peak is centred at ~ 772 nm with a full width at half maximum (FWHM) of 42 nm. The peak intensity is higher than that for the perovskite films prepared using a onestep method since both the film-nanorods structure and the large substrate coverage contribute to increasing the photon extraction efficiency. The absorption spectrum shows that the onset occurs at ~ 780 nm, consistent with previous reports.[13,21,22]

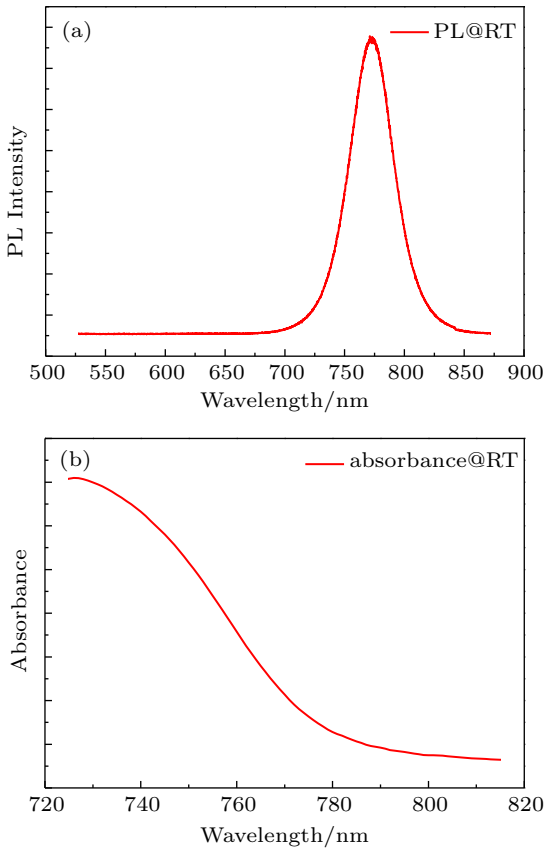


Fig. 3. (color online) (a) The PL spectrum of $CH_3NH_3PbI_{3-x}Cl_x$ at room temperature, with the peak at 772 nm. (b) The absorption spectrum of $CH_3NH_3PbI_{3-x}Cl_x$ at room temperature, with the onset position at ~ 780 nm.

To investigate the exciton binding energy and other photoluminescence characteristics, cryogenic PL measurements (10–300 K) were performed. Figure 4(a) shows that the PL

intensity varies with the measurement temperature. The spectra are complicated and can be categorised into three groups based on their features. Figure 4(b) shows the normalized PL intensities of $CH_3NH_3PbI_{3-x}Cl_x$ for temperatures in the 10–60 K range. These spectra have two peaks, which blue shift with an increase in the temperature. During the process, the relative intensity of the peaks on the right gradually increases. It has been proven that organic–inorganic metal halide perovskite is in the orthorhombic phase at low temperatures.[23] After fitting, the spectra were actually found to contain three peaks (1.53 eV, 1.58 eV, and 1.66 eV at 10 K), as shown in Fig. 5(a). Figure 4(c) shows how the normalized PL intensity of $CH_3NH_3PbI_{3-x}Cl_x$ changes as the temperature increases from 60 K to 140 K. The lower-energy peak gradually moves rightward, with the FWHM decreasing from 115 meV to 43 meV. Meanwhile, a red shift occurs while the right peak remains at $\sim$ 1.66 eV. The relative intensity of the right peak gradually decreases until the peak vanishes.

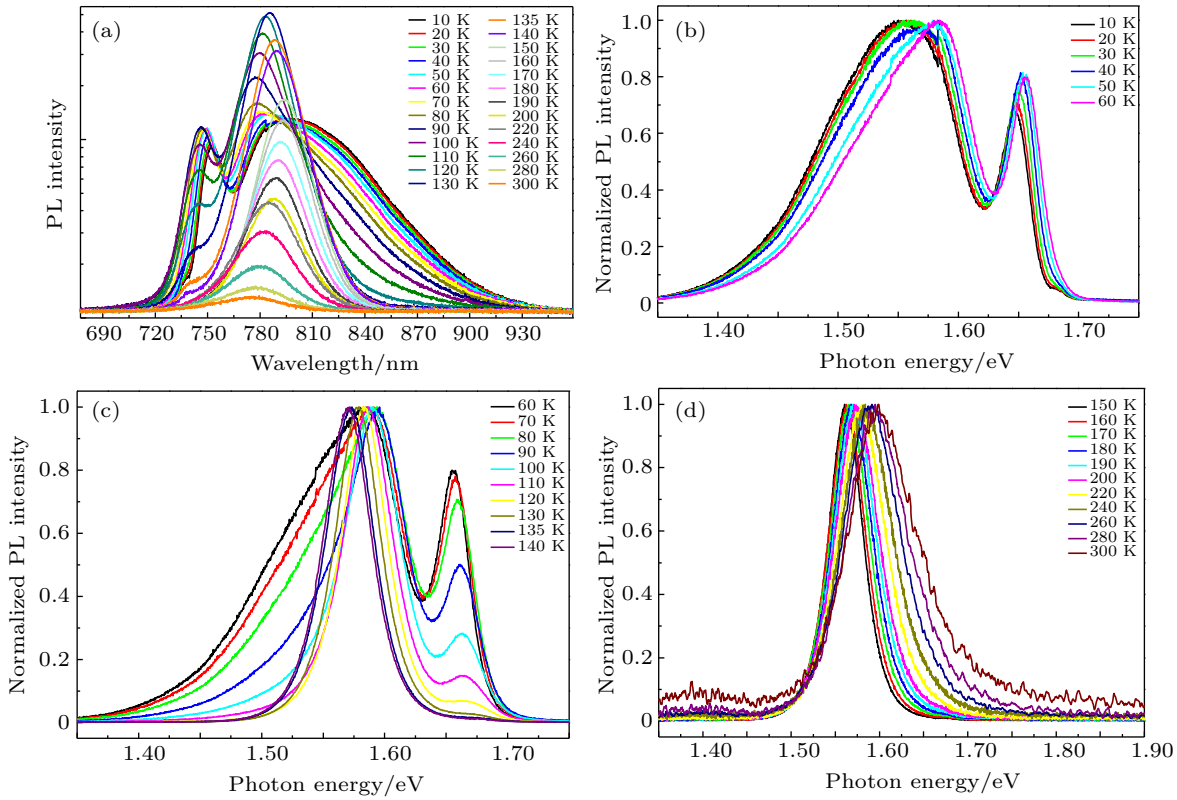


Fig. 4. (color online) (a) Temperature-dependent PL spectra of $CH_3NH_3PbI_{3-x}Cl_x$, for temperatures in the 10–300 K range. (b) Normalized PL spectra for temperatures in the 10–60 K range. (c) Normalized PL spectra for temperatures in the 60–150 K range. (d) Normalized PL spectra, for temperatures in the 150–300 K range.

To explain these phenomena, we decomposed the spectra by fitting the peaks, and found that the spectra contained three peaks (peak 1, peak 2 and peak 3), as shown in Fig. 5. In general, the structural transition from the orthorhombic phase to the tetragonal phase involved two peaks. However, as is well known, the characteristics can be influenced by many factors, for example the preparation method and the characterisation conditions. $CH_3NH_3PbI_{3-x}Cl_x$ is an organic–inorganic hybrid material, in which the organic and the inorganic parts are linked by hydrogen bonds. We speculate that temperature variation changed the bounds in our samples. The interaction between the organic and inorganic parts changed the hybrid band structure, which might have led to the appearance of peak 1. Peaks 2 and 3 reflect the structural transition from the orthorhombic phase to the tetragonal phase. Peak 2 is due to the luminescence in the tetragonal phase while peak 3 is due to the luminescence in the orthorhombic phase. As the temperature increases from 60 K to 140 K, the intensity of peak 1 slowly decreases while that of peak 2 increases. However, both peaks shift by $\sim$ 1.56 eV. This explains why the lower-energy peak in Fig. 4(c) exhibits a red shift. The peak at $\sim$ 1.66 eV becomes broader and weaker as the temperature increases from 10 K to 140 K. We speculate that during the process, the unit cell volume expands increasing the crystal strain as the temperature increases thus increasing the exciton-phonon interaction, which results in the peak broadening. At 140 K, only one peak remains; thus, $CH_3NH_3PbI_{3-x}Cl_x$ is officially transformed from the lowtemperature orthorhombic phase into the high-temperature tetragonal phase, consistent with other reports.[24–26]

Figure 4(d) shows the normalized PL spectra for temperatures in the 150–300 K range. For temperatures above

140 K, the peak moves toward higher energies, with a steady tetragonal phase. It is believed that when the temperature increases, the vibration energy of atoms increases, therefore increasing the interatomic distance. When the interatomic distance increases, the potential energy of electrons decreases which can decrease the width of the bandgap. However, in this process, as the interatomic distance increases, the overlap between electron clouds decreases, which can narrow the energy band and increase the band gap. Clearly, the latter mechanism plays a more important part in the temperaturedependent process which is similar to what occurs in some lead salt semiconductors.[27]

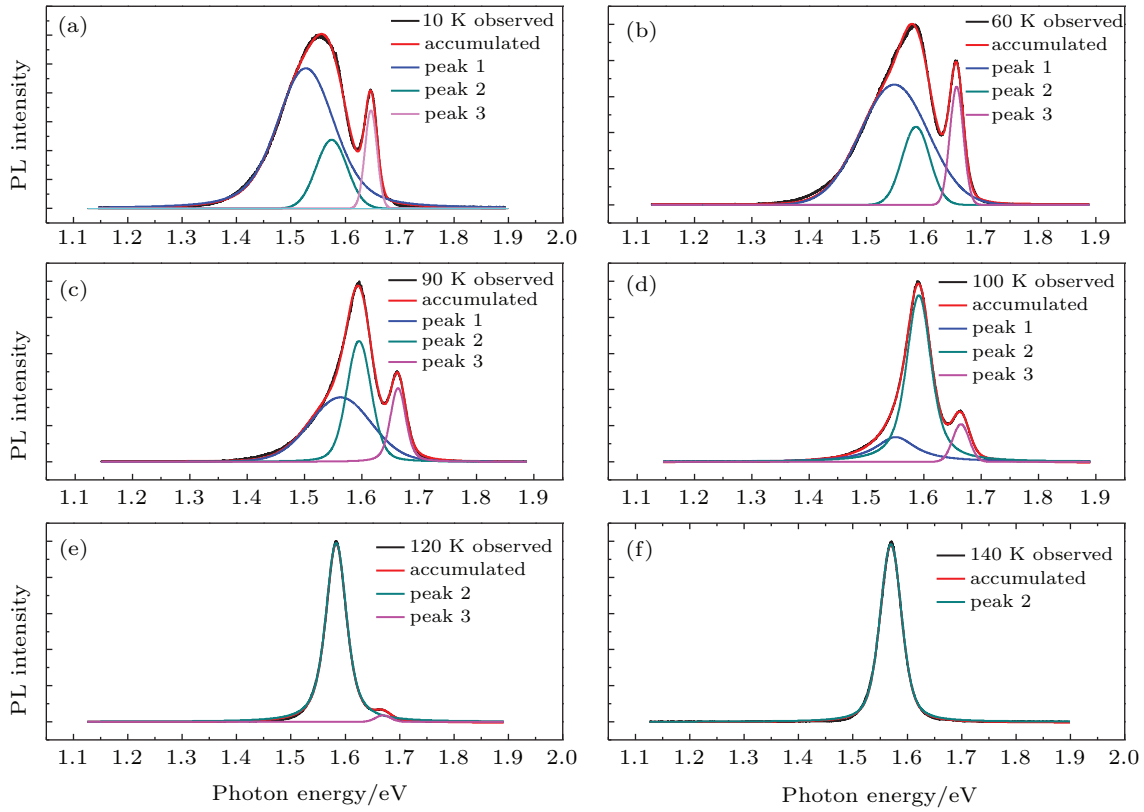


Fig. 5. (color online) Evolution of the three peaks that make up the main two original peaks, for temperatures in the 10–140 K range ((a)–(f)). Peaks 1, 2, 3 were obtained by peak fitting.

For these conditions, we calculated typical physical parameters, such as the exciton binding energy, to study the temperature dependence of the luminescence of perovskite films, which is shown in Fig. 6(a).

As is well known, the relationship between the integrated PL intensity and temperature can be described by the following Arrhenius equation:

$$I = \frac{I_0}{1 + A\,\mathrm{e}^{-E_\mathrm{B}/k_\mathrm{B}T}}, \tag{1}$$

in which I_0 is the integrated PL intensity at 0 K, k_B is the Boltzmann constant (8.617×10^{-5} eV/K), E_B is the exciton binding energy, A is the fitting constant, and T represents the measurement temperature.

Using this method, the exciton energy was calculated as 77.6 ± 10.9 meV, which is a little higher than previously reported values for solution-processed perovskites.[26,28] According to Tom Wu *et al.*, this may be owing to the doping of Cl atoms which can contribute to hindering the separation of excitons and increasing the exciton binding energy.[28] This suggests that our preparation method of $CH_3NH_3PbI_{3-x}Cl_x$ may yield significant Cl doping.

The broadening of these PL peaks can be described using the boson model,

$$\Gamma(T) = \Gamma_0 + \sigma T + \frac{\Gamma_\mathrm{op}}{\mathrm{e}^{-\hbar\omega_\mathrm{op}/k_\mathrm{B}T} - 1} \tag{2}$$

in which Γ_0 is the inhomogeneous broadening term, and σ and Γ_op capture the interactions of excitons with acoustic phonons and optical phonons, respectively. At low temperatures, the frequency of optical phonons is higher than that of acoustic phonons which makes it difficult for the optical phonons to scatter. At higher temperatures, the number of optical phonons involved in the interactions increases. Owing to this, in this regime, the acoustic phonons do not contribute to the peak broadening as much as the optical phonons.

The fit parameters are indicated on the plot. That is, the first and the second terms in the broadening equation are dominant at low temperatures, but the first item is roughly constant. Consequently, for temperatures in the 150–300 K range the

second term can be neglected, and the equation becomes

$$\Gamma(T) = \Gamma_0 + \frac{\Gamma_{\rm op}}{{\rm e}^{-\hbar\omega_{\rm op}/k_{\rm B}T} - 1}. \quad (3)$$

The width broadening and the energy of optical phonons were estimated as $\Gamma_{\rm op} = 189.2 \pm 52.1$ meV and $E_{\rm op} = 38.8 \pm 2.5$ meV, in a good agreement with previously reported values.[29]

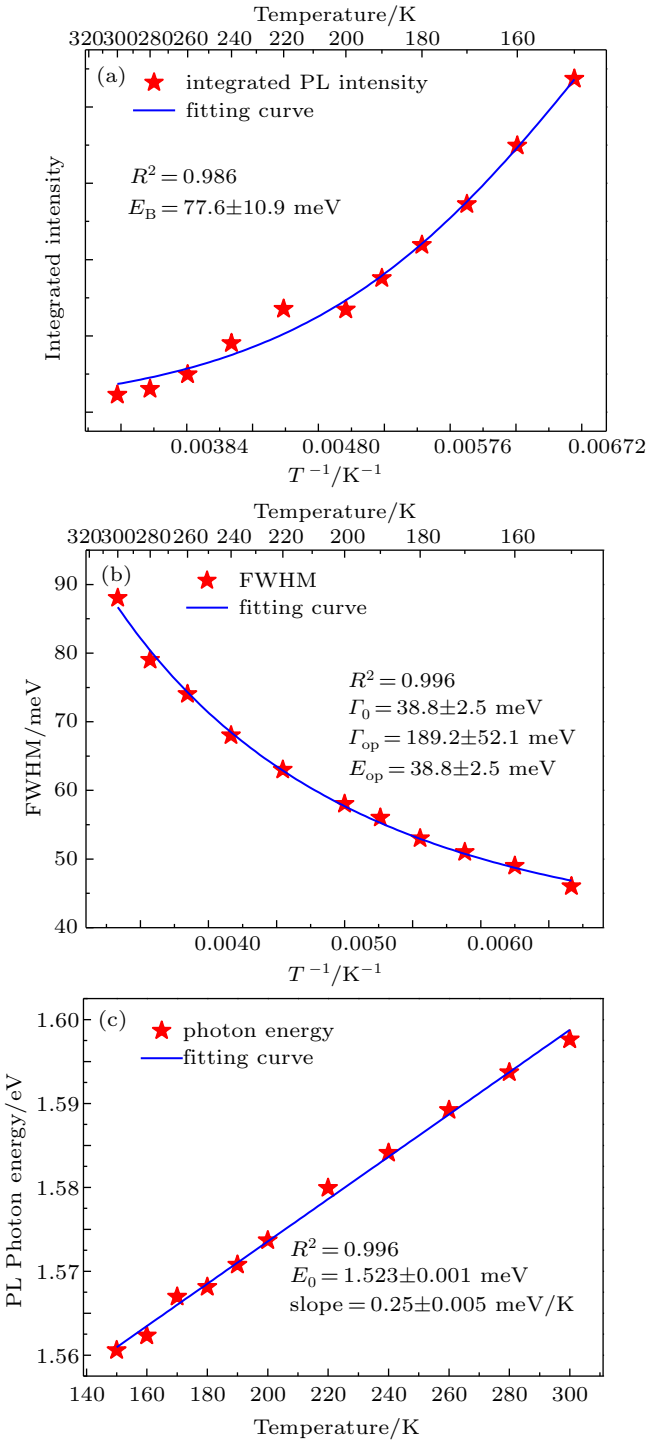


Fig. 6. (color online) (a) Integrated PL intensity vs. temperature, and the Arrhenius equation fit, for temperatures in the 150–300 K range. The calculated exciton energy is 77.6 ± 10.9 meV. (b) PL peak FWHM vs. temperature, and a non-linear fit using the boson model. The fit parameters are indicated on the plot. (c) Photon energy vs. temperature, and a linear fit.

In addition, we calculated the temperature coefficient of the perovskite film, for temperatures in the 150–300 K range, for the data in Fig. 6(c). The data exhibit the slope corresponding to a blue shift, with the temperature coefficient of 0.25 meV/K which is obviously large. Clearly the linear temperature coefficient can help to decide the peak position at a specific temperature to some extent.

4. Conclusion

In summary, the perovskite $CH_3NH_3PbI_{3-x}Cl_x$ films were prepared using a two-step method. Analysis of the films' surface morphology revealed large crystals and substrate coverage. The luminescence characteristics of temperature-dependent PL spectra were studied for temperatures in the 10–300 K range. The phase transition temperature from the low-temperature orthorhombic phase to the high-temperature tetragonal phase was $\sim$ 140 K. The exciton binding energy was 77.6 ± 10.9 meV. The optical phonon energy was 38.8 ± 2.5 meV. These data provide important optical information about perovskite $CH_3NH_3PbI_{3-x}Cl_x$ and about the family of organic-inorganic metal halide perovskites. This information can serve as a reference for designing perovskite-based optoelectronic devices.

References

[1] Xing G, Mathews N, Lim S S, Yantara N, Liu X, Sabba D, Gratzel M, Mhaisalkar S and Sum T C 2014 *Nat. Mater.* **13** 476
[2] Oga H, Saeki A, Ogomi Y, Hayase S and Seki S 2014 *J. Am. Chem. Soc.* **136** 13818
[3] Kuppler R J, Timmons D J, Fang Q R, Li J R, Makal T A, Young M D, Yuan D Q, Zhao D, Zhuang W J and Zhou H C 2009 *Coordin. Chem. Rev.* **253** 3042
[4] Plank N O V, Howard I, Rao A, Wilson M W B, Ducati C, Mane R S, Bendall J S, Louca R R M, Greenham N C, Miura H, Friend R H, Snaith H J and Welland M E 2009 *J. Phys. Chem. C* **113** 18515
[5] Bi D Q, Wu F, Qu Q Y, Yue W J, Cui Q, Shen W, Chen R Q, Liu C W, Qiu Z L and Wang M T 2011 *J. Phys. Chem. C* **115** 3745
[6] Chen Q Y, Huang Y, Huang P R, Ma T, Cao C and He Y 2016 *Chin. Phys. B* **25** 027104
[7] Li J F, Zhao C, Zhang H, Tong J F, Zhang P, Yang C Y, Xia Y J and Fan D W 2016 *Chin. Phys. B* **25** 028402
[8] Kojima K T A, Shirai Y and Miyasaka T 2009 *J. Am. Chem. Soc.* **131** 6050
[9] Zhang T K, Yu T and Zou Z G 2015 *Physics* **44** 315
[10] Jeon N J, Noh J H, Yang W S, Kim Y C, Ryu S, Seo J and Seok S I 2015 *Nature* **517** 476
[11] Hu X, Zhang X D, Liang L, Bao J, Li S, Yang W L and Xie Y 2014 *Adv. Funct. Mater.* **24** 7373
[12] Fang H H, Raissa R, Abdu-Aguye M, Adjokatse S, Blake G R, Even J and Loi M A 2015 *Adv. Funct. Mater.* **25** 2378
[13] Tan Z K, Moghaddam R S, Lai M L, Docampo P, Higler R, Deschler F, Price M, Sadhanala A, Pazos L M, Credgington D, Hanusch F, Bein T, Snaith H J and Friend R H 2014 *Nat. Nanotechnol.* **9** 687
[14] Huang M H, Mao S, Feick H, Yan H Q, Wu Y Y, Kind H, Weber E, Russo R and Yang P D 2001 *Science* **292** 1897
[15] He T, Xia Y J, Qin H C, Guan Z S and Li W Y 2011 *Physics* **4** 0
[16] Yu X X, Zhou Y, Liu J, Jin H B, Fang X Y and Cao M S 2015 *Chin. Phys. B* **24** 127307
[17] Shi Z F, Zhang Y T, Cai X P, Wang H, Wu B, Zhang J X, Cui X J, Dong X, Liang H W, Zhang B L and Du G T 2014 *Cryst. Eng. Comm.* **16** 455

[18] Burschka J, Pellet N, Moon S J, Humphry-Baker R, Gao P, Nazeeruddin M K and Gratzel M 2013 *Nature* **499** 316

[19] Zheng L L, Ma Y Z, Chu S S, Wang S F, Qu B, Xiao L X, Chen Z J, Gong Q H, Wu Z X and Hou X 2014 *Nanoscale* **6** 8171

[20] Zheng L, Zhang D, Ma Y, Lu Z, Chen Z, Wang S, Xiao L and Gong Q 2015 *Dalton T.* **44** 10582

[21] Lee M M, Teuscher J, Miyasaka T, Murakami N T and Snaith H J 2012 *Science* **338** 643

[22] Jaramillo-Quintero O A, Sanchez R S, Rincon M and Mora-Sero I 2014 *J. Phys. Chem. Lett.* **6** 1883

[23] Wehrenfennig C, Liu M Z, Snaith H J, Johnston M B and Herz L M 2014 *APL Mater.* **2** 081513

[24] D'Innocenzo V, Grancini G, Alcocer M J P, Kandada A R S, Stranks S D, Lee M M, Lanzani G, Snaith H J and Petrozza A 2014 *Nat. Commun.* **5** 3586

[25] Kao T S, Chou Y H, Chou C H, Chen F C and Lu T C 2014 *Appl. Phys. Lett.* **105** 231108

[26] Savenije T J, Ponseca C S, Kunneman L, Abdellah M, Zheng K, Tian Y, Zhu Q, Canton S E, Scheblykin I G, Pullerits T, Yartsev A and Sundstrom V 2014 *J. Phys. Chem. Lett.* **5** 2189

[27] Georgiev T and Baleva G L M 1990 *J. Phys.: Condens. Matter* **1** 2935

[28] Wu K, Bera A, Ma C, Du Y M, Yang Y, Li L and Wu T 2014 *Phys. Chem. Chem. Phys.* **16** 22476

[29] Quarti C, Grancini G, Mosconi E, Bruno P, Ball J M, Lee M M, Snaith H J, Petrozza A and Angelis F D 2014 *J. Phys. Chem. Lett.* **5** 279